DOI: 10.1534/genetics.109.106419

MNR2 Regulates Intracellular Magnesium Storage in *Saccharomyces cerevisiae*

Nilambari P. Pisat, Abhinav Pandey[1] and Colin W. MacDiarmid[2]

Department of Biology, University of Missouri, St. Louis, Missouri 63121-4400

Manuscript received June 25, 2009
Accepted for publication August 22, 2009

ABSTRACT

Magnesium (Mg) is an essential enzyme cofactor and a key structural component of biological molecules, but relatively little is known about the molecular components required for Mg homeostasis in eukaryotic cells. The yeast genome encodes four characterized members of the CorA Mg transporter superfamily located in the plasma membrane (Alr1 and Alr2) or the mitochondrial inner membrane (Mrs2 and Lpe10). We describe a fifth yeast CorA homolog (Mnr2) required for Mg homeostasis. *MNR2* gene inactivation was associated with an increase in both the Mg requirement and the Mg content of yeast cells. In Mg-replete conditions, wild-type cells accumulated an intracellular store of Mg that supported growth under deficient conditions. An *mnr2* mutant was unable to access this store, suggesting that Mg was trapped in an intracellular compartment. Mnr2 was localized to the vacuole membrane, implicating this organelle in Mg storage. The *mnr2* mutant growth and Mg-content phenotypes were dependent on vacuolar proton-ATPase activity, but were unaffected by the loss of mitochondrial Mg uptake, indicating a specific dependence on vacuole function. Overexpression of Mnr2 suppressed the growth defect of an *alr1 alr2* mutant, indicating that Mnr2 could function independently of the *ALR* genes. Together, our results implicate a novel eukaryotic CorA homolog in the regulation of intracellular Mg storage.

MAGNESIUM (Mg) is a critical factor in a wide variety of biological processes (Elin 1994), and there are at least 300 Mg-dependent enzymes (Williams 1993; Cowan 1995). Given its diverse roles in biology, understanding how cells maintain Mg homeostasis is of fundamental importance. Maintaining a consistent Mg concentration in the cytosol and organelles is likely to require tight regulation of passive influx, active efflux, and sequestration mechanisms. Despite the importance of these mechanisms, relatively little is known about the molecular identity, function, and regulation of Mg transporters in eukaryotic cells.

The yeast Alr1 and Alr2 proteins were the first eukaryotic Mg transporters identified. *ALR1* inactivation conferred Mg-dependent growth and blocked Mg uptake (MacDiarmid and Gardner 1998; Graschopf *et al.* 2001). The closely related ortholog Alr2 was not essential for growth, but could compensate for the loss of Alr1 when overexpressed and was found to physically associate with Alr1 *in vivo* (MacDiarmid and Gardner 1998; Wachek *et al.* 2006). Further studies identified two related proteins in the mitochondrial inner membrane (Mrs2 and Lpe10). Both proteins were required for the entry of Mg into the mitochondrial matrix, and loss-of-function mutations in either gene caused similar reductions in mitochondrial function and Mg content (Bui *et al.* 1999; Gregan *et al.* 2001a,b). All four of these proteins are members of the metal ion transporter (MIT) superfamily, the founder member of which is CorA from *Salmonella typhimurium* (Gardner 2003; Knoop *et al.* 2005). In general, MIT proteins mediate rapid, membrane-potential-dependent transport, suggesting that they form Mg-selective channels (MacDiarmid and Gardner 1998; Liu *et al.* 2002; Kolisek *et al.* 2003; Froschauer *et al.* 2004; Schindl *et al.* 2007). Although divergent in primary sequence, typical MIT proteins possess two conserved structural features: a pair of transmembrane domains close to the C terminus and a triad of conserved residues (glycine–methionine–asparagine) that are essential for Mg transport (Knoop *et al.* 2005). The low number of transmembrane domains predicted to be present in MIT proteins suggested that oligomerization was required for ion transport (Kolisek *et al.* 2003; Warren *et al.* 2004), and independent crystallographic studies of a CorA homolog from *Thermotoga maritima* support this model (Eshaghi *et al.* 2006; Lunin *et al.* 2006; Payandeh and Pai 2006). *T. maritima* CorA formed a homopentamer of subunits in which the C-terminal transmembrane domains clustered together to form a membrane-spanning pore. The N-terminal regions of the

Supporting information is available online at http://www.genetics.org/cgi/content/full/genetics.109.106419/DC1.

[1]*Present address:* Ranbaxy Research Laboratories, Research and Development Building III, Sector 18, plot number 20, Udyog Vihar Industrial Area, Gurgaon, Haryana-122001, India.

[2]*Corresponding author:* R424, Research Building, Department of Biology, University of Missouri, One University Blvd., St. Louis, MO 63121-4400. E-mail: macdiarmidc@umsl.edu

subunits formed a cytosolic "funnel" domain that incorporated several apparent Mg-binding sites, suggesting a regulatory role for this domain. Genetic studies provided evidence that the binding of Mg ions to these sites altered the conformation of the complex and decreased channel activity (Payandeh and Pai 2006; Payandeh *et al.* 2008). The activity of the Mrs2 protein was also shown to be dependent on Mg concentration (Schindl *et al.* 2007), suggesting that both prokaryotic and eukaryotic MIT proteins can respond directly to the cytosolic or matrix Mg concentration to promote homeostasis.

A fifth CorA homolog (*YKL064w*) is present in the yeast genome, but has not been characterized (MacDiarmid and Gardner 1998). The Ykl064w protein shares the two predicted transmembrane domains and conserved GMN motif characteristic of Mg-transporting members of the MIT family (MacDiarmid and Gardner 1998; Knoop *et al.* 2005). Phylogenetic analysis revealed that Ykl064w belongs to a subgroup of fungal MIT proteins in which a tryptophan residue replaces the conserved phenylalanine preceding the GMN motif (Knoop *et al.* 2005). Most sequenced yeast and fungal genomes include at least one Alr1 and one Ykl064w-type ortholog (Knoop *et al.* 2005). The presence of two discrete groups of fungal CorA proteins suggested that the Ykl064w-related proteins perform a novel function. For this reason, we decided to investigate the role of Ykl064w in ion homeostasis. Here we report that Ykl064w is a vacuolar membrane protein that is required for Mg homeostasis and present evidence implicating this protein in the regulation of intracellular Mg storage.

MATERIALS AND METHODS

Growth media and general methods: Yeast were routinely grown in YPD or SD medium with 2% glucose and required auxotrophic supplements [designated synthetic complete medium (SC)]. Low magnesium medium (LMM) was prepared using a commercial yeast nitrogen base mix lacking divalent cations (Q-Biogene). Divalent cations were added to give final concentrations of 1 mm $CaCl_2$, 0.15 μm $CuCl_2$, 0.75 μm $FeSO_4$, 2.5 μm $MnCl_2$, and 2.5 μm $ZnCl_2$. The Mg concentration of LMM was below levels detectable by atomic absorption spectroscopy (AAS; $<$ 10 nm). For some experiments, LMM was supplemented with $MgCl_2$ to give the concentration required or with 1 mm Na_2–EDTA to chelate trace amounts of Mg. Cell number per milliliter of yeast suspensions was determined by measuring the optical density at 595 nm (A_{595}) and comparing with a standard curve of A_{595} *vs.* viable cells. Yeast transformations were performed using standard methods (Gietz *et al.* 1992).

Plasmid construction: The plasmids pFL38, pFL44-S, pFL45-S (Bonneaud *et al.* 1991), and YCpALR1 (MacDiarmid and Gardner 1998) were described previously. To construct palr2TRP1, a 5-kb *Kpn*I genomic clone of *ALR2* in pBCSK$^-$ (Stratagene) was cut with *Bgl*II, and a 0.8-kb *Bgl*II fragment of pFL45-S containing the *TRP1* marker was inserted. All other plasmids constructed in this study were generated utilizing homologous recombination (Hua *et al.* 1997) between yeast plasmids gapped with restriction enzymes and PCR products amplified with high-fidelity DNA polymerase (EasyA polymerase, Stratagene). Correct plasmid construction was verified by DNA sequencing. The palr1HIS3 plasmid was constructed by the replacement of part of the *ALR1* ORF in YEpGALR1 (MacDiarmid and Gardner 1998) with a PCR-amplified *HIS3* gene via gap repair. pmnr2SpHIS5 was constructed by amplification of the *SpHIS5* gene from the pKT211 plasmid (Sheff and Thorn 2004), and its insertion within the *MNR2* ORF of YCpMNR2 via gap repair. YCpMNR2 was constructed by amplifying a 4.2-kb fragment of the *MNR2* gene (including the promoter and terminator regions) from genomic DNA of DY1457 and inserting this fragment into pFL38 via gap repair. The YEpGmycMNR2 plasmid was based on pMYC-Zap1$_{1\text{-}880}$ (Bird *et al.* 2000), which was modified by replacement of the *ZAP1* ORF with the amplified *MNR2* ORF via gap repair. The resulting construct contains five repeats of the *myc* epitope sequence fused to the second codon of the Mnr2 ORF. Expression of *myc*-Mnr2 from this plasmid is driven by the upstream activating sequence of the *GAL1* promoter fused to a minimal *CYC1* promoter (Bird *et al.* 2000). To generate YCpmycMNR2, the *myc*-Mnr2 ORF was amplified from YEpGmycMNR2 and used to repair the gapped YCpMNR2 plasmid, generating a low-copy construct in which the native *MNR2* promoter drives expression of *myc*-tagged Mnr2. To construct YCpCit-MNR2, a DNA fragment encoding a variant of yellow fluorescent protein [yEmCitrine, (Sheff and Thorn 2004)] was amplified from the pKT211 vector and inserted between the *myc* tags and the N-terminal end of the Mnr2 ORF in the YCpmycMNR2 plasmid. The function of all Mnr2 fusion proteins was verified by complementation of the Mg accumulation and growth phenotypes of an *mnr2* mutant strain (supporting information, Figure S1).

Yeast strain construction: *tfp1* and *mnr2 KAN^R* (KanMX4) diploid knockout mutant strains were obtained from Open Biosystems. DY1457 was described previously (Zhao and Eide 1996). Other strains used or constructed during this work are listed in Table 1. All introduced deletions were verified with PCR. To construct NP4, the *mnr2::KAN^R* locus and flanking DNA was amplified from genomic DNA of the diploid deletion mutant and transferred to DY1457 via transformation. To generate NP10, NP27, NP14, and NP20, DY1514 was sequentially transformed with the *mnr2::KAN^R* PCR product and the inserts of palr1HIS3 and palr2TRP1. The resulting diploid was sporulated to obtain clones of the appropriate genotypes. NP174, NP180, NP193, and NP201 were generated by sequential transformation of DY1514 with the insert of pmnr2SpHIS5 and a *tfp1::KAN^R* PCR product, followed by sporulation. NP103, NP107, and NP112 were derived by transformation of DBY747, and lpe10Δ-1 and mrs2Δ-2 (Gregan *et al.* 2001a) with the *mnr2::KAN^R* PCR product.

AAS and inductively coupled plasma-mass spectrometry: Measurement of total cell-associated Mg was routinely performed using AAS. Yeast cultures (5 ml) were harvested during exponential growth, collected by centrifugation, and washed twice with 1 mm Na_2–EDTA (pH 8.0) and twice with deionized water. Cells were resuspended in 1 ml of water and the A_{595} of each sample was recorded. One milliliter of each suspension was added to 1 ml of concentrated nitric acid in a 13-ml glass tube and digested by incubation for 16 hr at 95°. After addition of 2 ml 1× $LaCl_3$ buffer (10 mm $LaCl_3$, 240 mm HCl), each digest was adjusted to a total volume of 4 ml with purified water. Digests were diluted fivefold in 0.5× $LaCl_3$ buffer before measurement with a GBC 904AA instrument. Inductively coupled plasma-mass spectrometry (ICP–MS) analysis was performed essentially as previously described (Kim *et al.* 2004). Aliquots of yeast cultures (2–5 ml) were filtered through 0.45-μm nitrocellulose filters (Millipore) and washed twice with 5 ml of wash buffer (20 mm sodium citrate, pH 4, 1 mm EDTA) and once with 5 ml of Millipore water. The filters were digested with concentrated nitric acid before analysis. The contribution of the filters was subtracted from the final values, which were normalized to per-cell values as described for AAS.

TABLE 1

Yeast strains

Strain	Relevant genotype	Full genotype
DY1514	Wild-type	*MAT***a**/α *ade2/+ ade6/+ can1-100^{oc}/-his3-11,15/-leu2-3,112/-trp1-1/-ura3-52/-*
NP4	*mnr2*Δ	*MAT*α *ade6 can1-100^{oc} his3-11,15 leu2-3,112 trp1-1 ura3-52 mnr2::KAN^{R}*
NP10	*alr1*Δ	*MAT***a** *ade2 can1-100^{oc} his3-11,15 leu2-3,112 trp1-1 ura3-52 alr1::HIS3*
NP27	*alr2*Δ	*MAT***a** *can1-100^{oc} his3-11,15 leu2-3,112 trp1-1 ura3-52 alr2::TRP1*
NP14	*alr1*Δ *alr2*Δ	*MAT***a** *ade6 can1-100^{oc} his3-11,15 leu2-3,112 trp1-1 ura3-52 alr1::HIS3 alr2::TRP1*
NP20	*alr1*Δ *alr2*Δ *mnr2*Δ	*MAT***a** *ade2 can1-100^{oc} his3-11,15 leu2-3,112 trp1-1 ura3-52 alr1::HIS3 alr2::TRP1 mnr2::KAN^{R}*
NP174	Wild type	*MAT*α *ade2 can1-100^{oc} his3-11,15 leu2-3,112 trp1-1 ura3-52*
NP180	*mnr2*Δ	*MAT*α *ade2 can1-100^{oc} his3-11,15 leu2-3,112 trp1-1 ura3-52 mnr2::SpHIS5*
NP193	*tfp1*Δ	*MAT*α *ade2 can1-100^{oc} his3-11,15 leu2-3,112 trp1-1 ura3-52 tfp1::KAN^{R}*
NP201	*mnr2*Δ *tfp1*Δ	*MAT*α *ade2 can1-100^{oc} his3-11,15 leu2-3,112 trp1-1 ura3-52 mnr2::SpHIS5 tfp1::KAN^{R}*
DBY747	Wild type	*MAT***a** *his3-Δ1 leu2-3,112 ura3-52 trp1-289*
lpe10Δ-1	*lpe10*Δ	*MAT***a** *his3-Δ1 leu2-3,112 ura3-52 trp1-289 lpe10::URA3*
mrs2Δ-2	*mrs2*Δ	*MAT***a** *his3-Δ1 leu2-3,112 ura3-52 trp1-289 mrs2::SpHIS5*
NP103	*mnr2*Δ	*MAT***a** *his3-Δ1 leu2-3,112 ura3-52 trp1-289 mnr2::KAN^{R}*
NP107	*mnr2*Δ *lpe10*Δ	*MAT***a** *his3-Δ1 leu2-3,112 ura3-52 trp1-289 lpe10::URA3 mnr2::KAN^{R}*
NP112	*mnr2*Δ *mrs2*Δ	*MAT***a** *his3-Δ1 leu2-3,112 ura3-52 trp1-289 mrs2::SpHIS5 mnr2::KAN^{R}*

All strains were generated during this study except for DY1514 (obtained from David Eide), DBY747, mrs2Δ-2, and lpe10Δ-1 (obtained from Anton Graschopf). All strains are isogenic to DY1514 except for those isogenic to DBY747 (lpe10Δ-1, mrs2Δ-2, NP103, NP107, and NP112).

SDS–PAGE, immunoblotting, and microscopy: Crude protein extracts were prepared using a trichloroacetic acid extraction protocol (Ellis *et al.* 2004). SDS–PAGE and immunoblotting were performed using standard techniques (Harlow and Lane 1988), and immunoblots were developed using West Pico chemiluminescent substrate (Pierce Chemical). Antibodies for immunoblotting were obtained from Sigma-Aldrich, Molecular Probes, and Pierce Chemical. Indirect immunofluorescence microscopy was performed as previously described (MacDiarmid *et al.* 2000) by using a mouse α-*myc* primary (Abcam) and a goat anti-mouse secondary antibody labeled with Alexa Fluor 488 (Molecular Probes). FM4-64 staining of the vacuole membrane (Vida and Emr 1995) was performed by incubation of yeast cultures in medium containing 2 μM FM4-64 for 15 min. The cells were washed once in dye-free medium and then resuspended in fresh medium and incubated at 30° for 30 min to allow complete internalization of the dye. Fluorescence images were overlaid using Photoshop CS software (Adobe), which was also used to filter image noise and optimize contrast.

RESULTS

Effect of *YKL064w* on elemental content: Initial phenotypic characterization of a *ykl064w* deletion mutant revealed that this mutation was associated with a substantial increase in sensitivity to manganese ions and with a less severe sensitivity to calcium, zinc, and cobalt ions (Figure 1A). For this reason, the gene was designated *MNR2* (for **m**anga**n**ese **r**esistance). The potential role of Mnr2 in divalent cation homeostasis was further investigated by comparing the total elemental content of wild-type and *mnr2* strains after growth in a standard synthetic medium (+Mg values, Table 2). Although the *mnr2* mutation was associated with a moderate increase in phosphate and sulfur content, the largest effect was an elevated Mg content, suggesting that Mnr2 plays a role in Mg homeostasis. For this reason, we determined the effect of the mutation on growth and Mg content under Mg-deficient conditions (Figure 1, B and C). Somewhat surprisingly, the *mnr2* mutant showed a growth defect in Mg-deficient conditions (<100 μM Mg), due to a reduction in the initial growth rate (Figure 1B, inset). This growth defect did not appear to result from reduced Mg uptake under deficient conditions, as the elevated Mg content was most pronounced in these conditions (Figure 1C). Although a determination of the elemental content of Mg-deficient strains (Table 2) revealed a modest increase in the content of several cations in the *mnr2* mutant, the major effect of the mutation was a fivefold increase in Mg content, again supporting a specific role for Mnr2 in Mg homeostasis.

The higher Mg content of the *mnr2* mutant indicated that, unlike the Alr proteins, Mnr2 was not required for Mg uptake. For this reason, we suspected that this protein was involved in regulating access to an intracellular store of Mg. A previous study indicated that yeast accumulate excess Mg in Mg-replete conditions and can use this internal store of Mg to support growth in Mg-deficient conditions (Beeler *et al.* 1997). If the *mnr2* mutation prevented the utilization of this internal store, the mutant would retain Mg during growth in Mg-deficient conditions, resulting in an elevated Mg content. In addition, a lack of access to the store would be expected to inhibit growth of the mutant in Mg-deficient conditions. Experiments performed to test this model are described below.

Subcellular location of Mnr2: Studies of the distribution of Mg in yeast cells revealed a predominantly vacuolar location (Simm *et al.* 2007), implicating this

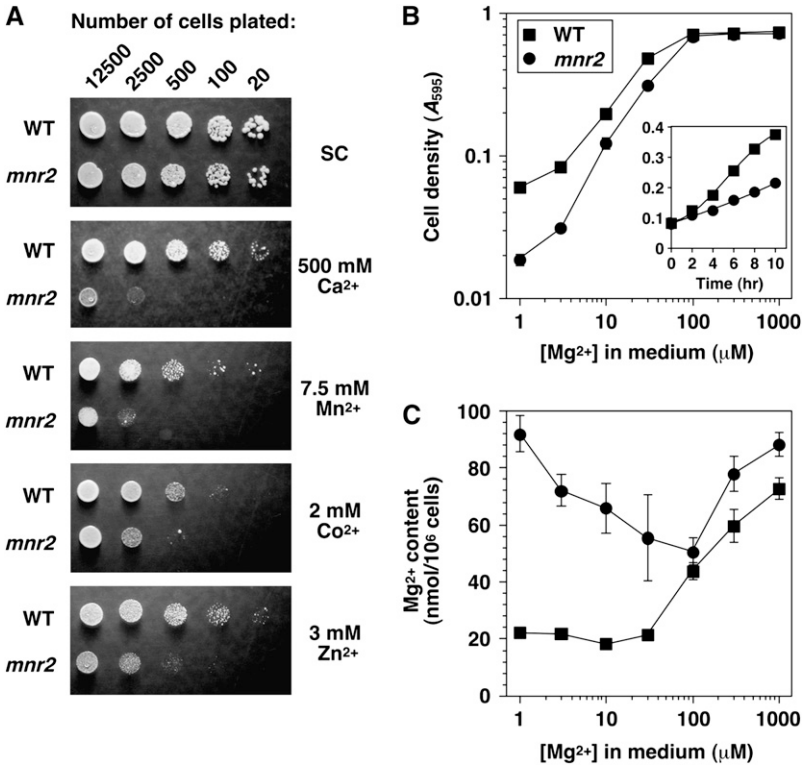

FIGURE 1.—The *mnr2* mutant shows defects in cation homeostasis. (A) Divalent cation sensitivity. Cultures of wild-type (DY1457) and *mnr2* (NP4) strains were grown to saturation, and the indicated number of cells were applied to SC−ura plates with no metal added (SC) or to SC−ura plates with metal ions added as chloride salts. Plates were incubated for 3 days before being photographed. (B) Mg requirement of wild-type (DY1457) and *mnr2* (NP4) strains. Aliquots of LMM containing the indicated concentration of Mg were inoculated to an A_{595} of 0.01 and incubated for 16 hr. Values for final cell density are shown (means of three replicates, ±1 SEM). (Inset) Growth curve of DY1457 and NP4 in LMM + 3 μM Mg. (C) Total cellular Mg content of wild-type (DY1457) and *mnr2* (NP4) yeast strains. Yeast cultures were grown in synthetic LMM containing the indicated concentration of Mg ions, and cell-associated Mg was assayed using AAS. Data points are the means of four independent replicates for DY1457 and of six independent replicates for NP4 (±1 SEM).

organelle in intracellular Mg storage. If Mnr2 is directly involved in regulating vacuolar Mg content, we would expect this protein to be located in the vacuolar membrane. We constructed a functional fusion of the YFP and Mnr2 proteins (Figure S1, A and B) and expressed it in a wild-type strain. YFP signal was predominantly observed in the vacuole membrane (Figure 2), the location of which was confirmed by staining with FM4-64 (VIDA and EMR 1995) (Figure 2, YFP-Mnr2/high Mg). FM4-64 clearly colocalized with YFP-Mnr2 (Figure 2, YFP-Mnr2/high Mg/Merge). In cells expressing untagged Mnr2, only diffuse autofluorescence was observed in the YFP channel (Figure 2, control/high Mg). Since Mnr2 contributed primarily to Mg homeostasis under deficient conditions, the location of the protein was also determined in cells depleted of Mg by 6 hr growth in Mg-deficient medium (Figure 2, YFP-Mnr2/low Mg). Under these conditions, cells displayed extensive vacuolar fragmentation, and large vacuoles were not clearly visible in DIC images. The YFP signal was distributed in small, clustered, ring-like structures that corresponded to the FM4-64 signal, consistent with

TABLE 2

Elemental content of wild-type and *mnr2* strains

Element	Wild type (+Mg)	*mnr2* (+Mg)	Fold change (+Mg)[a]	Wild type (−Mg)	*mnr2* (−Mg)	Fold change (−Mg)[a]
Mg	50.11 ± 2.52	84.16 ± 2.91	1.7	9.88 ± 0.79	53.14 ± 1.53	5.4
P	299.28 ± 7.84	423.41 ± 13.62	1.4	236.08 ± 9.59	464.96 ± 16.28	2.0
S	31.09 ± 5.17	46.31 ± 6.04	1.5	35.72 ± 2.66	35.96 ± 5.10	1.0
K	169.75 ± 4.90	184.81 ± 5.08	1.1	73.40 ± 3.75	169.44 ± 5.47	2.3
Ca	5.35 ± 0.37	6.58 ± 0.99	1.2	22.60 ± 0.58	43.43 ± 0.41	1.9
Mn	0.038 ± 0.004	0.047 ± 0.001	1.2	0.107 ± 0.006	0.189 ± 0.019	1.8
Fe	0.071 ± 0.009	0.068 ± 0.016	1.0	0.169 ± 0.037	0.242 ± 0.012	1.4
Co	0.387 ± 0.013	0.415 ± 0.015	1.1	0.499 ± 0.082	0.991 ± 0.060	2.0
Zn	1.46 ± 0.08	1.89 ± 0.18	1.3	2.23 ± 0.08	4.70 ± 0.17	2.1

Wild-type (NP174) and *mnr2* (NP180) strains were grown for 12 hr in LMM + 1 mM Mg (+Mg) or 1 μM Mg (−Mg), and elemental content was determined by ICP–MS analysis, as described in MATERIALS AND METHODS. Data are the mean of five replicates from two independent experiments. Units are nanomoles/10^6 yeast cells ± 1 SEM, except cobalt (picomoles/10^6 yeast cells). Only elements for which reproducible data were obtained are shown.

[a] Ratio of elemental content (*mnr2*/wild-type strain).

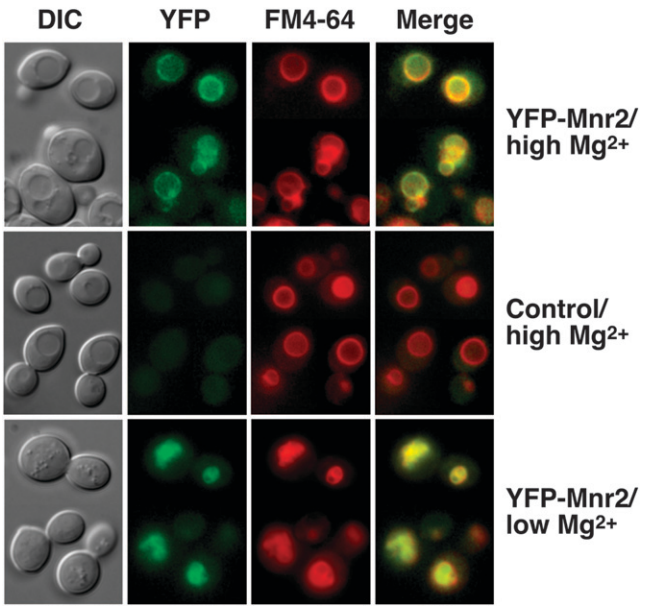

FIGURE 2.—Mnr2 is a vacuolar membrane protein. BY4743 cells expressing YFP-Mnr2 from a low-copy vector (YCpCitMNR2) or transformed with an empty vector (pFL38, control) were grown for 6 hr in LMM + 1 mM Mg (high Mg) or in LMM + 1 μM Mg (low Mg). Cells were treated with FM4-64 to visualize the vacuole membrane, and images were captured with the appropriate filter set (FM4-64 or YFP). Signal overlap is shown (Merge). DIC, differential interference contrast.

a vacuolar membrane location. Western blotting confirmed that the accumulation of Mnr2 was not affected by Mg deficiency (Figure S1, C). Thus, Mnr2 was expressed in both Mg-deficient and -replete cells, and it was present in the subcellular location appropriate to regulating vacuolar Mg content under both conditions.

Effect of the *mnr2* mutation on intracellular Mg stores: The effect of the *mnr2* mutation on Mg content suggested that Mnr2 might be required for the release of intracellular Mg stores under deficient conditions. To test this prediction, we first verified that intracellular Mg could support growth in the absence of external Mg. Wild-type and *mnr2* strains were grown in a medium with excess Mg (200 mM) to force excess Mg accumulation and generate "loaded" (L) cells or in a medium with a lower Mg content (30 μM) to generate cells with minimal Mg content ("nonloaded" or NL cells). Figure 1B illustrates that wild-type cells supplied with ≤30 μM Mg accumulated ~20 nmol Mg/10^6 cells. Since Mg content did not drop below this value when Mg supply was restricted further (Figure 1B), we believe that 20 nmol Mg/10^6 cells represents the minimum content of viable cells. For this reason, NL cells were expected to have minimal intracellular Mg stores. After 16 hr growth, L and NL cultures were transferred to LMM containing 1 mM EDTA to chelate trace amounts of Mg. Growth was monitored by change in cell density, and the use of stores was determined by measurement of Mg content. The results (Figure 3A) show that wild-type L cells grew significantly

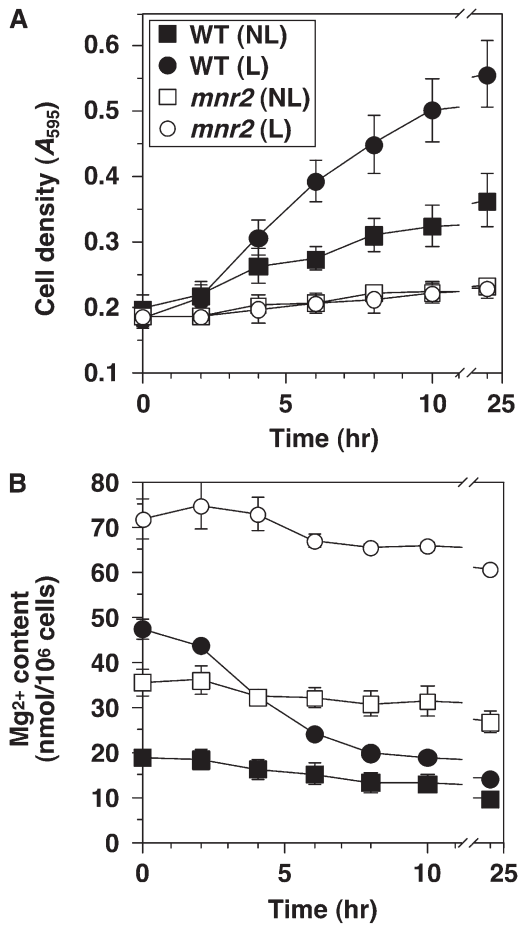

FIGURE 3.—The *mnr2* mutation prevents access to intracellular Mg stores. Cultures of wild-type (WT, DY1457) and *mnr2* (NP4) strains were grown to mid-log phase in LMM with 200 mM (loaded condition, L) or 30 μM Mg (nonloaded condition, NL), washed twice with 10 mM EDTA to remove extracellular Mg, and used to inoculate aliquots of LMM + 1 mM EDTA. LMM cultures were incubated at 30°, and samples were removed at the indicated times for determination of cell density (A) and Mg content (B). Error bars indicate ±1 SEM (three independent experiments).

faster than wild-type NL cells in Mg-free conditions. After 24 hr growth, wild-type L cells showed a 2.75-fold increase in cell density, compared to a 1.8-fold change for the NL cells. At the start of the experiment, the Mg content of L cells was >2-fold higher than NL cells (Figure 3B). In both wild-type cultures, Mg content decreased with growth, but L cells displayed a faster rate of decrease. For both L and NL cells, growth essentially ceased after 10 hr, at which time cellular Mg content was reduced to a similar low level (~15–20 nmol/10^6 cells). These observations confirm previous reports that intracellular Mg stores can be used to maintain growth in the absence of an external supply (BEELER *et al.* 1997) and further demonstrate that, under these conditions, the initial cell content of Mg determines the extent of growth.

We also examined the effect of the *mnr2* mutation on the ability to utilize excess intracellular Mg under Mg-

free conditions. At the start of the experiment, the Mg content of both L and NL *mnr2* cells was substantially higher than observed for the wild-type strain grown under equivalent conditions (Figure 3B). Nevertheless, this initial higher Mg content did not translate into a faster growth rate after transfer to Mg-free medium, as neither L nor NL *mnr2* cells grew significantly under these conditions (Figure 3A). Overall, these data indicate that the Mnr2 protein is essential for the utilization of excess intracellular Mg in the absence of an external source.

Genetic evidence for vacuolar Mg storage: *In vitro* studies indicated that Mg transport into vacuoles proceeded via a Mg^{2+}/H^+ antiport mechanism (Borrelly *et al.* 2001). Vacuolar proton-coupled exchangers utilize the proton gradient generated by the vacuolar H^+-ATPase (V-ATPase). Mutations that inactivated essential subunits of the V-ATPase reduced yeast Mg content (Eide *et al.* 2005), which is consistent with a dependence of the vacuolar Mg uptake system on this enzyme. If Mnr2 regulates the release of Mg from vacuolar stores, mutations that prevent vacuolar sequestration of Mg should suppress phenotypes associated with the *mnr2* mutation. To test this prediction, we determined the effect of combining the *tfp1* and *mnr2* mutations on Mg accumulation under Mg-replete and -deficient conditions (Figure 4A). *TFP1* encodes subunit A of the V1 domain of the V-ATPase, which is essential for the activity of this enzyme (Liu *et al.* 1997). Consistent with the above model, a *tfp1* mutant had a much lower Mg content than wild type after growth in Mg-replete conditions. The Mg content of the *tfp1* mutant was similar to that of Mg-deficient wild-type cells (~20 nmol/10^6 cells, Figure 1A and Figure 4A), which, as previously noted, represents the minimum Mg content of viable wild-type cells. In addition, there was little difference in Mg content between *tfp1* cells grown under Mg-replete or -deficient conditions, indicating that this mutant was unable to accumulate excess Mg. When *mnr2* and *tfp1* mutations were combined, the *tfp1* mutation completely suppressed the *mnr2* phenotype of elevated Mg content in deficient conditions. *TFP1* thus acts upstream of *MNR2* in a genetic pathway controlling intracellular Mg accumulation.

To investigate the effect of the *tfp1* mutation on Mg storage, we compared the growth of mutant strains in Mg-free medium, under which conditions all growth would be dependent on the utilization of excess intracellular Mg (Figure 4B). Consistent with its initial low Mg content, the *tfp1* mutant displayed a severe growth defect (Figure 4A). Growth of the *mnr2 tfp1* mutant was similar to that of the *tfp1* single mutant and less than that of the *mnr2* single mutant. These results again indicated that *TFP1* was epistatic to *MNR2* in a genetic pathway regulating Mg storage.

To investigate the specificity of this genetic interaction, we also determined the effect of combining the

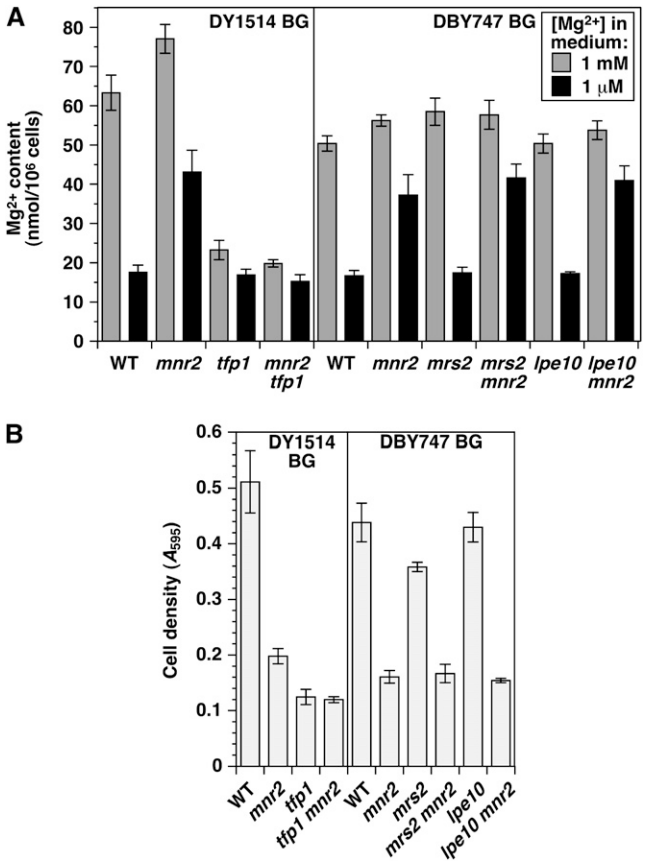

Figure 4.—Interaction of the *MNR2*, *TFP1*, *LPE10*, and *MRS2* genes. (A) Effect of *mnr2*, *tfp1*, *mrs2*, and *lpe10* mutations on Mg content. Wild-type (WT, DY1457), *mnr2* (NP4), *tfp1* (NP193), and *mnr2 tfp1* (NP201) strains isogenic to DY1514 (DY1514 BG) or wild-type (WT, DBY747), *lpe10* (lpe10Δ-1), *mrs2* (mrs2-Δ2), *mnr2 lpe10* (NP107), and *mnr2 mrs2* (NP112) strains isogenic to DBY747 (DBY747 BG) were cultured in LMM + 1 mM or 1 μM Mg for 16 hr, and Mg content was determined by AAS. Error bars indicate ±1 SEM (three replicates for DY1457-derived strains, five replicates for DBY747-derived strains). (B) Effect of the *mnr2*, *tfp1*, *mrs2*, and *lpe10* mutations on growth in Mg-free conditions. Strains described in A were cultured in SC medium, washed free of Mg, and used to inoculate aliquots of Mg-free LMM to an initial A_{595} of 0.1. After 16 hr incubation, cell density was recorded. Error bars indicate ±1 SEM (three replicates).

mnr2 mutation with deletions of genes encoding other organelle Mg transporters (Figure 4A). Previous reports indicated that both the Mrs2 and the Lpe10 proteins were essential for Mg uptake by mitochondria, as *lpe10* and *mrs2* mutants displayed a similar decrease in mitochondrial Mg content (Gregan *et al.* 2001a; Kolisek *et al.* 2003). To determine the effect of these mutations on whole-cell Mg content, we grew strains carrying combinations of *mnr2*, *lpe10*, and *mrs2* mutations in Mg-replete and -deficient conditions. Unlike the *tfp1* mutation, the *lpe10* and *mrs2* mutations did not reduce total cellular Mg content, suggesting that mitochondrial Mg is a relatively minor component of total cellular Mg. In addition, neither the *lpe10* nor the *mrs2* mutations

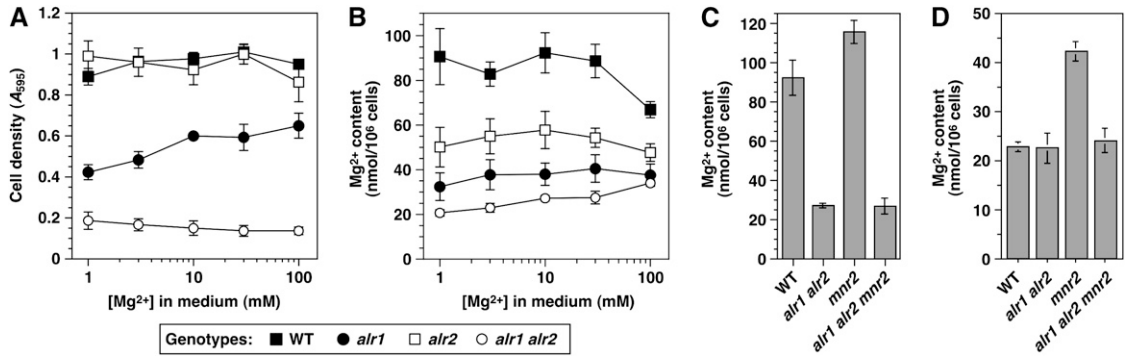

FIGURE 5.—Interaction of the *MNR2*, *ALR1*, and *ALR2* genes. (A and B) Cultures of wild-type (WT, DY1457), *alr1* (NP10), *alr2* (NP27), and *alr1 alr2* (NP14) strains were grown to saturation in YPD + 250 mM Mg, washed, and used to inoculate aliquots of LMM with the indicated Mg concentration to an initial A_{595} of 0.01. After 16 hr incubation, cell density of the cultures was determined (A), and cell-associated Mg content was measured via AAS (B). (C and D) Cultures of WT (DY1457), *mnr2* (NP4), *alr1 alr2* (NP14), and *alr1 alr2 mnr2* (NP20) strains were grown to saturation in YPD + 250 mM Mg, washed, and used to inoculate aliquots of LMM containing 10 mM Mg (C) or 1 μM Mg (D). After 16 hr growth, Mg content was determined using AAS. For all graphs, error bars indicate ±1 SEM (three independent experiments).

affected the severity of the *mnr2* Mg-content phenotype, indicating that Mnr2 does not regulate the Mg content of the mitochondrial compartment. In addition, there was no reproducible effect of the *lpe10* or *mrs2* mutations on growth in Mg-deficient conditions, either alone or in combination with the *mnr2* mutation (Figure 4B), indicating that the mitochondrial compartment does not make a significant contribution to the intracellular storage of excess Mg.

Interaction of the *ALR* and *MNR2* genes: To determine the relative contribution of the *ALR1*, *ALR2*, and *MNR2* genes to Mg homeostasis, we determined their combined effect on growth and Mg content (Figure 5). Several studies have suggested that *ALR2* does not contribute to Mg homeostasis in S288C-derived strains (MACDIARMID and GARDNER 1998; WACHEK *et al.* 2006; DA COSTA *et al.* 2007). However, *ALR1* inactivation had a less severe effect on viability in a W303-derived strain (TRAN *et al.* 2000), suggesting that *ALR2* was functional in this genetic background. Our experiments with W303-derived strains (DY1514 and isogenic derivatives) appeared to support a role for Alr2. When a set of *alr* mutant strains was grown over a range of Mg concentrations (Figure 5A), the *alr1* mutation inhibited growth, while the *alr2* mutation alone had no effect. However, combining the two mutations enhanced the *alr1*-associated growth defect, supporting a function for Alr2. In addition, whereas growth of the *alr1* single mutant was enhanced by supplementation with excess Mg, supplementation had no effect on the growth of the double mutant, consistent with a more severe block of Mg uptake in this strain. When Mg content of the strains was determined under the same conditions, both the *alr1* and the *alr2* mutants displayed reductions, but the double mutant had the lowest content (Figure 5B), again indicating that both Alr proteins contribute to Mg uptake. In summary, these data indicate that, in the W303 genetic background, inactivation of both Alr proteins is required to most effectively block Mg uptake.

We then determined the effect of combining the *alr1*, *alr2*, and *mnr2* mutations on Mg content. As previously observed (Table 2), the *mnr2* mutation increased Mg content under Mg-replete conditions (Figure 5C). However, when the *mnr2* mutation was combined with the *alr1* and *alr2* mutations, its effect on Mg content was eliminated. Complete suppression of the *mnr2* phenotype by the *alr1/2* mutations was also observed when the effect of the *mnr2* mutation was accentuated by Mg starvation (Figure 5D). The observation that the *ALR* genes are epistatic to *MNR2* is consistent with the dependence of intracellular Mg storage on access to an abundant supply of Mg. Our data indicate that, even when supplied with excess Mg, *alr1 alr2* mutants accumulated ~20 nmol Mg/10^6 cells (Figure 5C), which, as previously noted, represents the minimum Mg content of viable cells. For this reason, *alr1 alr2* mutant strains are unlikely to sequester a substantial quantity of Mg within intracellular stores, which would be expected to abrogate the effect of Mnr2.

Effect of *MNR2* overexpression in an *alr1 alr2* background: If Mnr2 is capable of directly mediating Mg transport, we reasoned that redirecting some of this protein to the plasma membrane might increase Mg influx, which could suppress phenotypes associated with the loss of Alr1/2 protein activity. To determine if the overexpression of Mnr2 would mislocalize the protein, the *myc*-Mnr2 ORF was expressed from a galactose-inducible promoter, and the subcellular location of the protein was determined using indirect immunofluorescence (Figure 6A). Although *myc*-Mnr2 was primarily associated with the vacuole membrane, a novel signal was also detected at the periphery of the cells (arrowheads in Figure 6A), suggesting accumulation in the plasma membrane. Although this peripheral staining

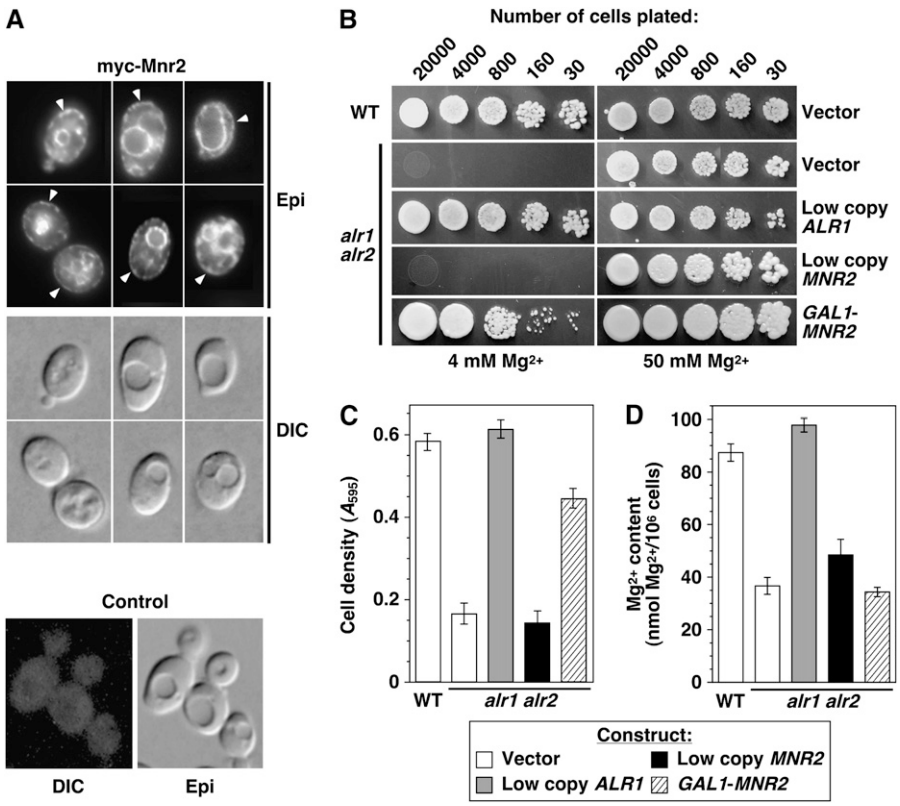

FIGURE 6.—*MNR2* overexpression in an *alr1 alr2* mutant. (A) Subcellular distribution of overexpressed *myc*-Mnr2. A wild-type strain (DY1514) was transformed with YEpGmycMNR2 (*myc*-Mnr2) or pFL38 (control). Cultures were grown to exponential phase in SC−ura + 2% galactose medium and processed for indirect immunofluorescence. Arrowheads indicate *myc*-Mnr2 signal at the cell periphery. (B). Wild-type (WT, DY1457) and *alr1 alr2* (NP14) strains were transformed with vector control (pFL38), low-copy *ALR1* (YCpALR1), low-copy *MNR2* (YCpmyc*MNR2*), or *GAL1* promoter-driven *MNR2* (YEpGmyc*MNR2*) constructs. Strains were grown in SD−ura medium with 100 mM Mg, and the indicated number of cells was applied to SC−ura plates + 2% galactose with a standard (4 mM) or high (50 mM) Mg concentration. Plates were incubated for 2 days before photography. (C and D) Strains described in A were grown to saturation in SC−ura supplemented with 100 mM Mg, washed twice with water, and used to inoculate aliquots of SC−ura with 2% galactose (4 mM Mg) to an initial A_{595} of 0.1. After 16 hr growth, final A_{595} was recorded (C), and Mg content was determined using AAS (D). For C and D, error bars indicate ±1 SEM (four independent experiments).

might also indicate an ER location, the absence of a distinct signal at the nuclear membrane means that the overall pattern was more consistent with a plasma membrane location.

To determine the phenotypic effect of this change, we assayed growth of the Mnr2-overexpressing *alr1 alr2* mutant and control strains under nonpermissive (standard synthetic medium with 2% galactose) and permissive conditions (the same medium supplemented with excess Mg) (Figure 6B). Either normal expression of Alr1 (using a low-copy *ALR1* genomic clone) or overexpression of *myc*-Mnr2 (*GAL1-MNR2*) restored growth of the mutant strain under nonpermissive conditions. Suppression by Mnr2 was dependent on a high level of expression, as the introduction of a low-copy *MNR2* genomic clone had no effect (Figure 6B, low-copy *MNR2*). To quantify this effect, growth curves were performed by culturing the same set of strains in standard synthetic medium with 4 mM Mg (Figure 6C). After 16 hr incubation, the wild-type and complemented strains completed ~2.5 doublings, while the noncomplemented strain grew very little (~0.25 doublings). In comparison, the cell number of the suppressed strain doubled twice in the same period of time. Thus, Mnr2 overexpression partially suppressed the growth defect of the *alr1 alr2* mutant.

We also examined the effect of Mnr2 overexpression on the Mg content of the *alr1 alr2* mutant (Figure 6D). The low Mg phenotype of this mutant was fully complemented by the expression of Alr1. However, overexpressing *myc*-Mnr2 did not increase Mg content above the level seen in a noncomplemented control strain. The implications of this observation will be examined further in the DISCUSSION, but, in general, the experiments shown in Figure 6 demonstrate that Mnr2 overexpression partially compensated for the loss of Alr protein activity.

DISCUSSION

Model for Mnr2 function in yeast: The data reported here add significantly to our understanding of fundamental processes of Mg homeostasis in eukaryotic cells, as illustrated in Figure 7. In part, this model proposes that, in Mg-replete conditions, an intracellular compartment (most probably the vacuole) provides a storage site for excess Mg. Consistent with this idea, the vacuolar Mg concentration is approximately fourfold higher than the cytoplasmic concentration in Mg-replete yeast cells (SIMM *et al.* 2007). The accumulation of excess Mg in the vacuole would require active transport to overcome the charge gradient generated by V-ATPase activity. Although the transporter responsible has not been identified, several studies have identified Mg^{2+}/H^{+} antiport activities in the vacuole membrane (OKOROKOV *et al.* 1985; BORRELLY *et al.* 2001). Mutations that inactivate V-ATPase activity (*e.g.*, *tfp1*) substantially re-

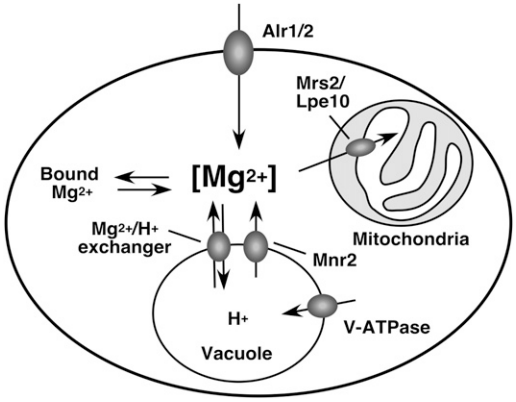

Figure 7.—Model for Mg homeostasis in yeast. Under Mg-replete conditions, Mg enters the cell via the Alr1 and Alr2 proteins to maintain the concentration of an essential cytosolic pool ($[Mg^{2+}]$). Excess cytosolic Mg is sequestered in the vacuole via an as-yet-unidentified proton-coupled Mg transporter, the activity of which is dependent on the proton gradient generated by V-ATPase. Under Mg-deficient conditions, these vacuolar Mg stores contribute to the maintenance of the cytosolic Mg concentration via the activity of Mnr2. The inactivation of Mnr2 prevents the release of Mg from the vacuole, which maintains vacuolar Mg content and inhibits growth under Mg-deficient conditions by restricting the supply of Mg to the cytosolic compartment.

duced total Mg content of yeast (Figure 4A) (Eide *et al.* 2005), as would be expected if these mutations inhibit proton-coupled Mg transport. However, it should be noted that the *tfp1* mutant phenotype of reduced Mg content may not represent a direct effect of a reduction in Mg^{2+}/H^+ exchanger activity, as this phenotype could result from the inhibition of other processes that may influence Mg accumulation in this compartment, such as polyphosphate synthesis (Beeler *et al.* 1997; Simm *et al.* 2007).

The model also proposes that vacuolar stores of Mg can be utilized to offset cytosolic Mg deficiency. Previous work (Beeler *et al.* 1997) as well as our observations (Figure 3) show that the initial Mg content of wild-type yeast cells affects the rate of growth upon transfer to Mg-free medium and that Mg content rapidly decreases under these conditions. Because ~80% of the Mg content of replete cells is vacuolar (Simm *et al.* 2007), these observations suggest that, when replete cells are transferred to deficient conditions, vacuolar Mg is redistributed to maintain the required concentration in other critical cellular compartments. The effect of the *tfp1* mutation on Mg content and the severe growth defect displayed by *tfp1* cells transferred to Mg-deficient conditions (Figure 4B) provide support for this view. In addition, several lines of evidence indicate that Mnr2 is required for the release of vacuolar Mg. Although an *mnr2* mutant strain accumulated more Mg than a wild-type strain during growth in Mg-replete conditions, this increased content had no effect on the subsequent growth of the mutant under deficient conditions (Figure 3). The growth defect exhibited by the *mnr2* mutant under these conditions suggests that an essential Mg-dependent compartment (such as the cytosol) was Mg deficient. The opposite effect of the *mnr2* and *alr1/alr2* mutations on Mg content (Figure 5) and the location of the Mnr2 protein (Figure 2) is consistent with Mnr2 supplying this essential compartment with Mg from vacuolar stores, rather than from the external environment. Indirect evidence for a direct role of Mnr2 in Mg transport came from the observation that Mnr2 overexpression appeared to relocate a fraction of the protein to the cell surface, while also partially suppressing the growth defect of an *alr1 alr2* mutant (Figure 6, B and C). Although this experiment did not provide direct evidence for Mg transport by Mnr2, it did demonstrate that Mnr2 could still function in the absence of the Alr proteins, suggesting that Mnr2 does not simply act as a regulatory or structural component of these proteins. This ability appears to distinguish Mnr2 from a class of yeast transporter orthologs that do not mediate solute transport, functioning instead as cell-surface receptors. For example, the Rgt2 and Snf3 proteins are glucose receptors required for a signal transduction pathway that regulates glucose transporter expression. Although both are orthologs of the Hxt glucose transporters, neither gene could suppress the growth defect of an *hxt1-7*Δ mutant deficient in glucose uptake, even when overexpressed (Ozcan *et al.* 1998). Finally, *myc* and YFP-tagged versions of Mnr2 were detected in both Mg-replete and -deficient cells, and YFP-tagged Mnr2 accumulated in the vacuole membrane of deficient cells (Figure 2, Figure S1), indicating that Mnr2 is present in the correct location under the appropriate conditions to directly regulate the Mg content of the vacuole.

Several other lines of evidence support general aspects of this model. First, the inhibition of proton-coupled secondary transport systems in the vacuole by the inactivation of Tfp1 suppressed the *mnr2* phenotype of increased Mg accumulation (Figure 4A), as would be expected if Tfp1 is required for the initial accumulation of Mg in the vacuole, and Mnr2 determines the Mg content of the vacuole by regulating its release from this organelle. The dependence of Mg storage on V-ATPase activity was also supported by the severe effect of the *tfp1* mutation on growth in Mg-free medium (Figure 4B), which indicates the absence of Mg stores in this strain. Second, eliminating Mg uptake into mitochondria had no effect on the severity of the *mnr2* Mg-accumulation phenotype, indicating that the *mnr2* mutation did not cause a general overaccumulation of Mg within all intracellular compartments. Finally, Mnr2 function was dependent on the efficient accumulation of excess Mg; when a severe block in Mg uptake was imposed by the inactivation of both the Alr proteins (Figure 5), the high Mg content phenotype of the *mnr2* mutation was suppressed. Together, these observations are consistent with Mnr2 functioning to directly mediate the release

of Mg from a vacuolar compartment responsible for the storage of excess Mg.

Effect of Mnr2 overexpression on *alr1 alr2* phenotypes: One somewhat surprising finding of this work was that, although Mnr2 overexpression improved the growth of an *alr1 alr2* mutant, it did not restore the Mg content of the mutant to the level of a wild-type strain (Figure 6D). These observations are consistent with at least three explanations, as outlined below. First, the overexpression of Mnr2 might have facilitated growth by reducing the minimal Mg requirement of yeast cells (*i.e.*, without improving the supply or redistribution of Mg). A second possibility is that Mnr2 might have increased the rate of Mg release from the vacuole or the flux of Mg through this compartment, thus improving the Mg supply to the cytosol. In support of this model, we note that Mnr2 overexpression significantly increased its accumulation in the vacuole membrane (Figure 6A). Finally, it is possible that (as previously suggested) the redirection of a fraction of Mnr2 to the plasma membrane enabled a small increase in Mg uptake, thus compensating directly for the loss of the Alr proteins. This minor increase in Mg uptake may have provided sufficient Mg to improve growth, but not enough to completely refill intracellular stores and restore normal cellular Mg content. In support of this model, we note that Mnr2 overexpression did not completely restore wild-type growth (Figure 6C), which, together with its low Mg content, suggests that the suppressed strain remained Mg deficient. However, the data presented here do not yet allow us to definitively distinguish between these three models, and more work is required to determine if the Mnr2 protein can directly mediate Mg transport.

Mg homeostasis and elemental content of yeast: In addition to the effect of the *mnr2* mutation on Mg, we also observed other changes in elemental content related to Mg homeostasis (Table 2). In both wild-type and *mnr2* strains, variation in Mg content was associated with altered phosphate content. Previous reports have also noted a close relationship between Mg supply and phosphate accumulation by yeast (Weimberg 1975; Beeler *et al.* 1997; Simm *et al.* 2007). The basis for this correlation is still unclear, however, and further work is required to understand the relationship. In addition to this effect, Mg supply also altered the accumulation of micronutrient metal ions. Wild-type yeast cultured in Mg-deficient conditions had a higher calcium, manganese, cobalt, and zinc content than Mg-replete cells (Table 2). We suggest that this effect may reveal the influence of extracellular Mg concentration on the influx of divalent cations via a Mg-inhibited, low-affinity uptake system. The existence of such a system in yeast is supported by several previous reports. For example, the restriction of Mg supply enhanced the sensitivity of *Saccharomyces cerevisiae* and *Schizosaccharomyces pombe* to manganese, nickel, and cobalt (Joho *et al.* 1991; Blackwell *et al.* 1997, 1998; Eitinger *et al.* 2000), consistent with these cations competing with Mg for the same low-affinity transport system. Several studies have linked this low-affinity uptake system to the Alr1 and Alr2 proteins and their homologs. The overexpression of either Alr1 or Alr2 conferred sensitivity to calcium, manganese, cobalt, zinc, and nickel ions and enhanced cobalt uptake (MacDiarmid and Gardner 1998), while the mutation of an Alr1 homolog from *S. pombe* increased nickel and zinc tolerance (Eitinger *et al.* 2000; Sarikaya *et al.* 2006). If fungal Alr homologs are capable of accumulating divalent cations other than Mg, the availability of Mg may also influence divalent cation accumulation via changes in gene expression. Both the level of *ALR1* mRNA and the stability of the Alr1 protein were reported to increase under Mg-deficient conditions (Graschopf *et al.* 2001). In Mg-deficient cells, elevated Alr1 expression might further enhance divalent cation accumulation, perhaps accounting for the enhanced sensitivity of Mg-starved yeast to manganese ions (Blackwell *et al.* 1997, 1998). Mg deficiency might also directly upregulate the activity of the Alr proteins. Although little is known about Alr1 regulation, the activity of bacterial and yeast CorA proteins is coupled to Mg^{2+} availability via the operation of a Mg-sensing domain located in the cytosol or mitochondrial matrix (Schindl *et al.* 2007; Payandeh *et al.* 2008), and a similar mechanism may operate for the Alr proteins.

Elemental analysis also revealed that, under Mg-deficient conditions, the *mnr2* mutation was associated with an increased content of calcium, manganese, cobalt, and zinc. If the Alr proteins do play a role in divalent cation uptake, this phenotype suggests that their activity and/or expression might be increased in *mnr2* strains. A mechanism for this effect is suggested by the observation that Alr1 and Alr2 expression may be regulated by Mg supply (Graschopf *et al.* 2001; Wachek *et al.* 2006), which in turn may be determined by Mnr2 activity. An upregulation of the Alr systems might also explain the divalent cation sensitivity of *mnr2* strains (Table 2 and Figure 1A). To test this model, we are currently studying the effect of Mg supply and the *mnr2* mutation on Alr1 expression and activity.

Vacuolar Mg storage in higher eukaryotes: One important implication of this work is that the homologs of Mnr2 in higher eukaryotes may also play a role in regulating intracellular Mg storage. Differentiated plant cells contain large vacuoles that may play an important role in the storage of inorganic nutrients [reviewed in Martinoia *et al.* (2007)], and tonoplast membranes can mediate active transport of Mg (Amalou *et al.* 1992, 1994), suggesting that Mg could be sequestered in these organelles. Most plant genomes encode multiple MIT proteins (Schock *et al.* 2000; Li *et al.* 2001). The Arabidopsis plasma membrane protein AtMGT1 (Li *et al.* 2001), the chloroplast inner membrane protein AtMrs2-11 (Drummond *et al.* 2006), and the mitochon-

drial protein AtMgt5 (Chen *et al.* 2009) have all been shown to play important roles in Mg homeostasis, but the function of many other members of this large gene family remains unknown. The identification of a functional homolog of Mnr2 in plants would further advance our understanding of Mg homeostasis in higher eukaryotes as well as provide a potentially useful tool to manipulate the nutrient content of economically important species.

The authors thank Amanda Bird, David Eide, Richard Gardner, and Anton Graschopf for supplying yeast strains and plasmids; David Eide, Bethany Zolman, Wendy Olivas, and Christopher Wolin for comments on the manuscript; James O'Brien for assistance with AAS; and David Salt for assistance with ICP–MS. This work was supported by a Research Award from the University of Missouri-St. Louis.

LITERATURE CITED

Amalou, Z., R. Gibrat, C. Brugidou, P. Trouslot and J. d'Auzac, 1992 Evidence for an amiloride-inhibited $Mg^{2+}/2H^+$ antiporter in lutoid (vacuolar) vesicles from latex of *Hevea brasiliensis*. Plant Physiol. **100:** 255–260.

Amalou, Z., R. Gibrat, P. Trouslot and J. D'Auzac, 1994 Solubilization and reconstitution of the $Mg^{2+}/2H^+$ antiporter of the lutoid tonoplast from *Hevea brasiliensis* latex. Plant Physiol. **106:** 79–85.

Beeler, T., K. Bruce and T. Dunn, 1997 Regulation of cellular Mg^{2+} by *Saccharomyces cerevisiae*. Biochim. Biophys. Acta **1323:** 310–318.

Bird, A. J., H. Zhao, H. Luo, L. T. Jensen, C. Srinivasan *et al.*, 2000 A dual role for zinc fingers in both DNA binding and zinc sensing by the Zap1 transcriptional activator. EMBO J. **19:** 3704–3713.

Blackwell, K. J., J. M. Tobin and S. V. Avery, 1997 Manganese uptake and toxicity in magnesium-supplemented and unsupplemented *Saccharomyces cerevisiae*. Appl. Microbiol. Biotechnol. **47:** 180–184.

Blackwell, K. J., J. M. Tobin and S. V. Avery, 1998 Manganese toxicity towards *Saccharomyces cerevisiae*: dependence on intracellular and extracellular magnesium concentrations. Appl. Microbiol. Biotechnol. **49:** 751–757.

Bonneaud, N., O. Ozier-Kalogeropoulos, G. Y. Li, M. Labouesse, L. Minvielle-Sebastia *et al.*, 1991 A family of low and high copy replicative, integrative and single-stranded *S. cerevisiae/E. coli* shuttle vectors. Yeast **7:** 609–615.

Borrelly, G., J. C. Boyer, B. Touraine, W. Szponarski, M. Rambier *et al.*, 2001 The yeast mutant *vps5*D affected in the recycling of Golgi membrane proteins displays an enhanced vacuolar Mg^{2+}/H^+ exchange activity. Proc. Natl. Acad. Sci. USA **98:** 9660–9665.

Bui, D. M., J. Gregan, E. Jarosch, A. Ragnini and R. J. Schweyen, 1999 The bacterial magnesium transporter CorA can functionally substitute for its putative homologue Mrs2p in the yeast inner mitochondrial membrane. J. Biol. Chem. **274:** 20438–20443.

Chen, J., L. G. Li, Z. H. Liu, Y. J. Yuan, L. L. Guo *et al.*, 2009 Magnesium transporter AtMGT9 is essential for pollen development in Arabidopsis. Cell Res. **19:** 887–898.

Cowan, J. A., 1995 Introduction to the biological chemistry of the magnesium ion, pp. 1–23 in *The Biological Chemistry of Magnesium*, edited by J. A. Cowan. VCH Publishers, New York.

da Costa, B. M., K. Cornish and J. D. Keasling, 2007 Manipulation of intracellular magnesium levels in *Saccharomyces cerevisiae* with deletion of magnesium transporters. Appl. Microbiol. Biotechnol. **77:** 411–425.

Drummond, R., A. Tutone, Y. Li and R. Gardner, 2006 A putative magnesium transporter AtMRS2-11 is localized to the plant chloroplast envelope membrane system. Plant Sci. **170:** 78–89.

Eide, D. J., S. Clark, T. M. Nair, M. Gehl, M. Gribskov *et al.*, 2005 Characterization of the yeast ionome: a genome-wide analysis of nutrient mineral and trace element homeostasis in *Saccharomyces cerevisiae*. Genome Biol. **6:** R77.

Eitinger, T., O. Degen, U. Bohnke and M. Muller, 2000 Nic1p, a relative of bacterial transition metal permeases in *Schizosaccharomyces pombe*, provides nickel ion for urease biosynthesis. J. Biol. Chem. **275:** 18029–18033.

Elin, R. J., 1994 Magnesium: the fifth but forgotten electrolyte. Am. J. Clin. Pathol. **102:** 616–622.

Ellis, C. D., F. Wang, C. W. MacDiarmid, S. Clark, T. Lyons *et al.*, 2004 Zinc and the Msc2 zinc transporter protein are required for endoplasmic reticulum function. J. Cell Biol. **166:** 325–335.

Eshaghi, S., D. Niegowski, A. Kohl, D. Martinez Molina, S. A. Lesley *et al.*, 2006 Crystal structure of a divalent metal ion transporter CorA at 2.9 angstrom resolution. Science **313:** 354–357.

Froschauer, E. M., M. Kolisek, F. Dieterich, M. Schweigel and R. J. Schweyen, 2004 Fluorescence measurements of free $[Mg^{2+}]$ by use of MagFura-2 in *Salmonella enterica*. FEMS Microbiol. Lett. **237:** 49–55.

Gardner, R. C., 2003 Genes for magnesium transport. Curr. Opin. Plant Biol. **6:** 263–267.

Gietz, R. D., A. St. Jean, R. A. Woods and R. H. Schiestl, 1992 Improved method for high efficiency transformation of intact yeast cells. Nucleic Acids Res. **8:** 1425.

Graschopf, A., J. A. Stadler, M. K. Hoellerer, S. Eder, M. Sieghardt *et al.*, 2001 The yeast plasma membrane protein Alr1 controls Mg^{2+} homeostasis and is subject to Mg^{2+}-dependent control of its synthesis and degradation. J. Biol. Chem. **276:** 16216–16222.

Gregan, J., D. M. Bui, R. Pillich, M. Fink, G. Zsurka *et al.*, 2001a The mitochondrial inner membrane protein Lpe10p, a homologue of Mrs2p, is essential for magnesium homeostasis and group II intron splicing in yeast. Mol. Gen. Genet. **264:** 773–781.

Gregan, J., M. Kolisek and R. J. Schweyen, 2001b Mitochondrial Mg^{2+} homeostasis is critical for group II intron splicing *in vivo*. Genes Dev. **15:** 2229–2237.

Harlow, E., and D. Lane, 1988 *Antibodies: A Laboratory Manual*. Cold Spring Harbor Laboratory Press, Cold Spring Harbor, NY.

Hua, S. B., M. Qiu, E. Chan, L. Zhu and Y. Luo, 1997 Minimum length of sequence homology required for *in vivo* cloning by homologous recombination in yeast. Plasmid **38:** 91–96.

Joho, M., K. Tarumi, M. Inouhe, H. Tohoyama and T. Murayama, 1991 Co^{2+} and Ni^{2+} resistance in *Saccharomyces cerevisiae* associated with a reduction in the accumulation of Mg^{2+}. Microbios **67:** 177–186.

Kim, D., J. L. Gustin, B. Lahner, M. W. Persans, D. Baek *et al.*, 2004 The plant CDF family member TgMTP1 from the Ni/Zn hyperaccumulator *Thlaspi goesingense* acts to enhance efflux of Zn at the plasma membrane when expressed in *Saccharomyces cerevisiae*. Plant J. **39:** 237–251.

Knoop, V., M. Groth-Malonek, M. Gebert, K. Eifler and K. Weyand, 2005 Transport of magnesium and other divalent cations: evolution of the 2-TM-GxN proteins in the MIT superfamily. Mol. Genet. Genomics **274:** 205–216.

Kolisek, M., G. Zsurka, J. Samaj, J. Weghuber, R. J. Schweyen *et al.*, 2003 Mrs2p is an essential component of the major electrophoretic Mg^{2+} influx system in mitochondria. EMBO J. **22:** 1235–1244.

Li, L., A. F. Tutone, R. S. Drummond, R. C. Gardner and S. Luan, 2001 A novel family of magnesium transport genes in *Arabidopsis*. Plant Cell **13:** 2761–2775.

Liu, G. J., D. K. Martin, R. C. Gardner and P. R. Ryan, 2002 Large Mg^{2+}-dependent currents are associated with the increased expression of *ALR1* in *Saccharomyces cerevisiae*. FEMS Microbiol. Lett. **213:** 231–237.

Liu, Q., X. H. Leng, P. R. Newman, E. Vasilyeva, P. M. Kane *et al.*, 1997 Site-directed mutagenesis of the yeast V-ATPase A subunit. J. Biol. Chem. **272:** 11750–11756.

Lunin, V. V., E. Dobrovetsky, G. Khutoreskaya, R. Zhang, A. Joachimiak *et al.*, 2006 Crystal structure of the CorA Mg^{2+} transporter. Nature **440:** 833–837.

MacDiarmid, C. W., and R. C. Gardner, 1998 Overexpression of the *Saccharomyces cerevisiae* magnesium transport system confers resistance to aluminum ion. J. Biol. Chem. **273:** 1727–1732.

MacDiarmid, C. W., L. A. Gaither and D. Eide, 2000 Zinc transporters that regulate vacuolar zinc storage in *Saccharomyces cerevisiae*. EMBO J. **19:** 2845–2855.

Martinoia, E., M. Maeshima and H. E. Neuhaus, 2007 Vacuolar transporters and their essential role in plant metabolism. J. Exp. Bot. **58:** 83–102.

Okorokov, L. A., T. V. Kulakovskaya, L. P. Lichko and E. V. Polorotova, 1985 H^+/ion antiport as the principal mecha-

nism of transport systems in the vacuolar membrane of the yeast *Saccharomyces carlsbergensis*. FEBS Lett. **192:** 303–306.

Ozcan, S., J. Dover and M. Johnston, 1998 Glucose sensing and signaling by two glucose receptors in the yeast *Saccharomyces cerevisiae*. EMBO J. **17:** 2566–2573.

Payandeh, J., and E. F. Pai, 2006 A structural basis for Mg^{2+} homeostasis and the CorA translocation cycle. EMBO J. **25:** 3762–3773.

Payandeh, J., C. Li, M. Ramjeesingh, E. Poduch, C. E. Bear *et al.*, 2008 Probing structure-function relationships and gating mechanisms in the CorA Mg^{2+} transport system. J. Biol. Chem. **283:** 11721–11733.

Sarikaya, A. T., G. Akman and G. Temizkan, 2006 Nickel resistance in fission yeast associated with the magnesium transport system. Mol. Biotechnol. **32:** 139–146.

Schindl, R., J. Weghuber, C. Romanin and R. J. Schweyen, 2007 Mrs2p forms a high conductance Mg^{2+} selective channel in mitochondria. Biophys. J. **93:** 3872–3883.

Schock, I., J. Gregan, S. Steinhauser, R. Schweyen, A. Brennicke *et al.*, 2000 A member of a novel *Arabidopsis thaliana* gene family of candidate Mg^{2+} ion transporters complements a yeast mitochondrial group II intron-splicing mutant. Plant J. **24:** 489–501.

Sheff, M. A., and K. S. Thorn, 2004 Optimized cassettes for fluorescent protein tagging in *Saccharomyces cerevisiae*. Yeast **21:** 661–670.

Simm, C., B. Lahner, D. Salt, A. LeFurgey, P. Ingram *et al.*, 2007 *Saccharomyces cerevisiae* vacuole in zinc storage and intracellular zinc distribution. Eukaryot. Cell **6:** 1166–1177.

Tran, H. G., D. J. Steger, V. R. Iyer and A. D. Johnson, 2000 The chromo domain protein Chd1p from budding yeast is an ATP-dependent chromatin-modifying factor. EMBO J. **19:** 2323–2331.

Vida, T. A., and S. D. Emr, 1995 A new vital stain for visualizing vacuolar membrane dynamics and endocytosis in yeast. J. Cell Biol. **128:** 779–792.

Wachek, M., M. C. Aichinger, J. A. Stadler, R. J. Schweyen and A. Graschopf, 2006 Oligomerization of the Mg^{2+}-transport proteins Alr1p and Alr2p in yeast plasma membrane. FEBS J. **273:** 4236–4249.

Warren, M. A., L. M. Kucharski, A. Veenstra, L. Shi, P. F. Grulich *et al.*, 2004 The CorA Mg^{2+} transporter is a homotetramer. J. Bacteriol. **186:** 4605–4612.

Weimberg, R., 1975 Polyphosphate levels in nongrowing cells of *Saccharomyces mellis* as determined by magnesium ion and the phenomenon of "Uberkompensation." J. Bacteriol. **121:** 1122–1130.

Williams, R. J. P., 1993 Magnesium: an introduction to its biochemistry, pp. 15–30 in *Magnesium and the Cell*, edited by N. J. Birch. Academic Press, San Diego.

Zhao, H., and D. Eide, 1996 The yeast *ZRT1* gene encodes the zinc transporter protein of a high-affinity uptake system induced by zinc limitation. Proc. Natl. Acad. Sci. USA **93:** 2454–2458.

Communicating editor: A. P. Mitchell

GENETICS

Supporting Information
http://www.genetics.org/cgi/content/full/genetics.109.106419/DC1

MNR2 Regulates Intracellular Magnesium Storage in *Saccharomyces cerevisiae*

Nilambari P. Pisat, Abhinav Pandey and Colin W. MacDiarmid

DOI: 10.1534/genetics.109.106419

GENETICS

Supporting Information
http://www.genetics.org/cgi/content/full/genetics.109.106419/DC1

MNR2 Regulates Intracellular Magnesium Storage in *Saccharomyces cerevisiae*

Nilambari P. Pisat, Abhinav Pandey and Colin W. MacDiarmid

DOI: 10.1534/genetics.109.106419

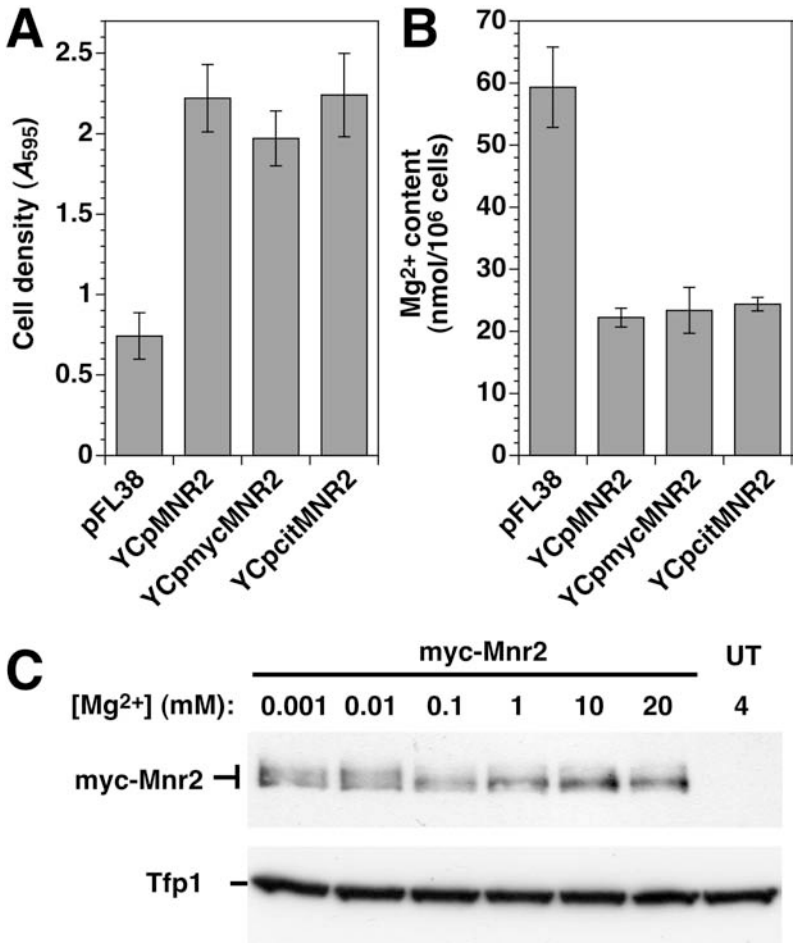

FIGURE S1.—Function and detection of Mnr2 protein fusions. An *mnr2* mutant strain (NP4) was transformed with a low copy empty vector (pFL38), untagged *MNR2* (YCpMNR2), myc-tagged *MNR2* (YCpmyc-MNR2), or YFP-tagged *MNR2* (YCpcit-MNR2), and the resulting strains grown in LMM-ura with 3 mM Mg for 16 h prior to determination of cell density (A) and total cellular Mg content (measured with AAS) (B). Data points are the average of four replicates from two independent experiments, error bars = +/- 1 SEM. (C) Detection of myc-Mnr2 by Western blotting. Cultures of DY1457 transformed with YCpmyc-MNR2 were grown in LMM-ura containing the indicated concentrations of Mg. Total protein was extracted and separated using SDS-PAGE and the myc-Mnr2 and Tfp1 proteins detected by immunoblotting. Protein extracted from a wild-type (DY1457) strain transformed with YCpMNR2 (untagged, UT) was included to control for antibody specificity.